The Mechanisms of Resistance Spot Welding of Magnesium to Steel

L. LIU, L. XIAO, J.C. FENG, Y.H. TIAN, S.Q. ZHOU, and Y. ZHOU

A novel technology has been developed for the resistance spot welding (RSW) of magnesium to steel producing joint strength as high as 95 pct of that of Mg to a Mg joint. The mechanisms of the dissimilar joining have been investigated using mechanical testing and metallurgical examination employing scanning electron microscopy, energy-dispersive X-ray spectroscopy, and X-ray diffraction. The results show that the mechanisms of joining during RSW of a magnesium alloy to Zn-coated steel involve braze welding, solid-state bonding, and soldering. The joint formation in comparison of RSW of Zn-coated steel with steel, Au-plated Ni, and bare Ni sheets is discussed. A possible expansion of this technology also is suggested.

DOI: 10.1007/s11661-010-0333-0

I. INTRODUCTION

THE continued efforts by automobile manufacturers to reduce vehicle weight have led to an increased use of high strength-to-weight-ratio magnesium alloys in the automobile architecture. Therefore, tasks of developing magnesium-to-magnesium similar joints and magnesium to others such as steel must be faced. The weldability of magnesium alloys by various methods, including laser,[1] friction stir,[2] laser-tungsten hybrid,[3] and resistance spot welding (RSW),[4] has been explored in detail. However, only a few studies have focused on the dissimilar joining of magnesium to steels. Butt joints[5] and overlap joints[6] of Mg to steel were performed by friction stir welding with a joint strength of around 70 pct of Mg base material and 3.7 kN (20 mm weld seam length), respectively. Laser-GTA (gas tungsten arc) hybrid welding was used to make overlap joints of Mg to steel.[7] However, it was hard to control these processes to avoid metallic oxides like MgO, ZnO, Fe_2O_3, or Al_2O_3,[5–7] which could reduce the strength of welds. The shear strength of dissimilar joints was improved from 56 pct to 100 pct of the base material by inserting a nickel interlayer.[8]

RSW is a primary joining method in the auto industry. If dissimilar joints could be performed successfully by RSW, then the costs could be attractive as a result of the lack of need for new equipment and the inherent low-cost characteristics of RSW. Limited publications have focused on characteristics of Mg/Mg similar RSW joints, such as nugget growth characteristics,[9] effects of surface conditions and welding parameters,[4,10] and solidification morphologies.[11] However, virtually no literature has been published on the RSW of Mg to steel. Only a few studies on RSW of Al to steel have been published.[12–15] Mg-free Al foil was inserted between Al and steel to suppress the formation of an intermetallic layer.[12] An Al layer was cold rolled to steel as a transition to aid the resistance welding process.[14] A laminate of steel and Al was inserted between Al and steel so the same types of metals could face each other.[15] The main problems of welding Al to steel using RSW are the formation of brittle intermetallic compounds, wetting of Al to steel, and large differences of electric conductivity and thermal physical properties between Al alloys and steel.[12,13] Some of these problems may be of concern as well in RSW of Mg to steel. The objectives of the current work were to develop an RSW process for welding magnesium alloy to DP600 steel and to investigate the mechanisms of the joining process using metallurgical examination and mechanical testing.

II. EXPERIMENTAL PROCEDURES

The materials used in this work were commercial-grade twin-roll strip cast Mg alloy AZ31B and zinc-coated DP600 steel sheets with thicknesses of 1.5 mm and 1.2 mm, respectively. Lap-welded joints were made by assembling test coupons that were cut to approximately 25 mm width and 100 mm length. Specimens were cut parallel to the rolling direction of the sheets and ultrasonically cleaned for 5 minutes in acetone. Prior to welding, the surfaces of the magnesium, coupons also were cleaned with a solution of 2.5 pct (wt/vol) chromic acid to minimize surface oxides because of their recognized negative effects on both weld strength and RSW electrode life.[4]

L. LIU, Ph.D. Candidate, is with the Department of Mechanical and Mechatronics Engineering, University of Waterloo, Waterloo N2L 3G1, Canada, and the State Key Laboratory of Advanced Welding Production Technology, Harbin Institute of Technology, Harbin 150001, P.R. China. L. XIAO, Ph.D. Candidate, and Y. ZHOU, Professor, are with the Department of Mechanical and Mechatronics Engineering, University of Waterloo. Contact e-mail: nzhou@mecheng1.uwaterloo.ca J.C. FENG, Professor, and Y.H. TIAN, Assistant Professor, are with the State Key Laboratory of Advanced Welding Production Technology, Harbin Institute of Technology. S.Q. ZHOU, Professor, is with the School of Mechanical Science and Engineering, Huazhong University of Science and Technology, Wuhan 430074, P.R. China.

Manuscript submitted December 5, 2009.
Article published online June 22, 2010

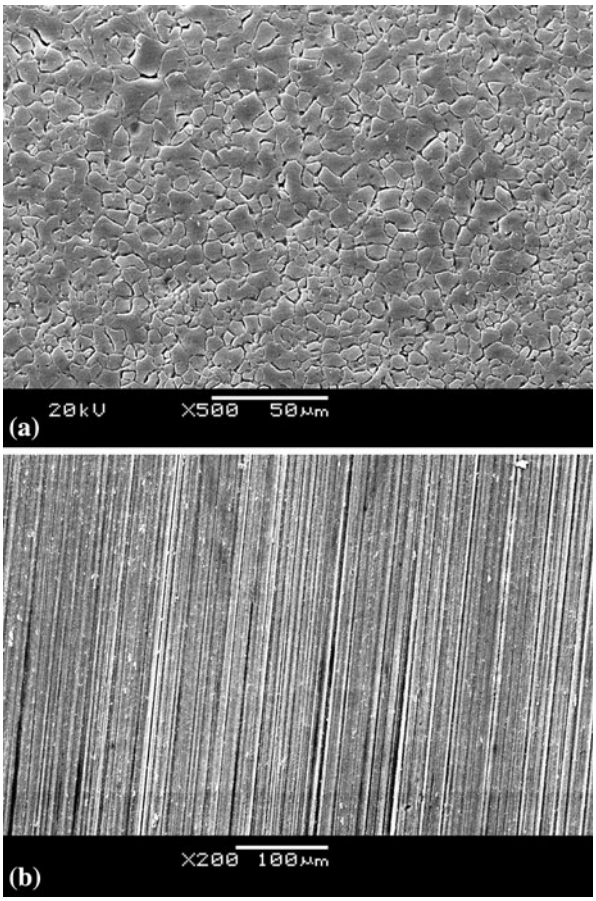

Fig. 1—AZ31 base material depicting the (*a*) microstructure and (*b*) the as-received surface.

The microstructure of AZ31B is shown in Figure 1(a). The AZ31 alloy consisted of equiaxed grains with an average grain size of 7.5 μm, measured according to ASTM E112-96. Rolling tracks are shown clearly on the surface of the AZ31B sheets (Figure 1(b)). An inspection of the DP600 steel microstructure with scanning electron microscopy (SEM) in Figure 2(a) showed the typical dual phase (DP) structure comprising martensite islands within the polygonal ferrite matrix. The surface of the DP600 steel was hot-dipped with zinc. The thickness of the zinc layer was about 9 μm to 12 μm measured by SEM (Figure 2(c)). Energy dispersive X-ray (EDX) showed the zinc layer contained 3 wt pct Fe and 97 wt pct Zn.

The specimens were welded using a median-frequency DC RSW machine (custom mode for University of Waterloo by Centerline Ltd, Windsor, Canada, Model No. 3005/T96302) in the constant current mode. A schematic diagram of the welding arrangement is shown in Figure 3. An electrode cap (FF25) with a sphere radius of 50.8 mm and face diameter of 16 mm, manufactured from a class Cu–Cr–Zr alloy, was used at the magnesium side, whereas a flat-face electrode was used at the steel side. The bulk resistance of magnesium is less than one third of steel (44.6 n$\Omega \times$ m for the magnesium alloy and 153 n$\Omega \times$ m for steel at 293 K (20 °C)),[9] and the thermal conductivity of AZ31B Mg alloy is 96 W/m $\times$ K,

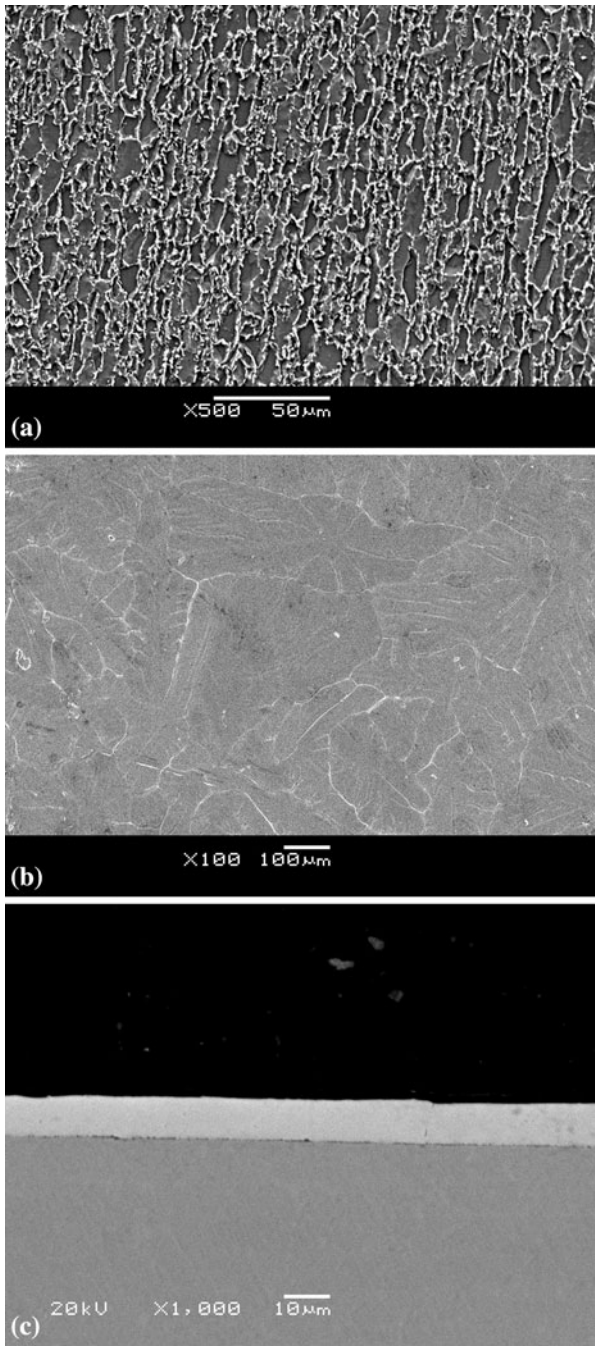

Fig. 2—DP600 steel base material depicting the (*a*) microstructure, (*b*) as-received surface, and (*c*) thickness of the Zn coating.

which is about twice that of steel. So, if symmetric tip contours were used to weld Mg to steel, then the heat generation and peak temperature at the steel side would be much higher than those on the magnesium side, which could induce the melting of steel, evaporation of magnesium, cracks, pores, and segregation in the fusion zone (nugget). Use of a domed electrode against the Mg surface and a flat electrode against the steel surface were planned to balance workpiece heating by reducing the current density and by increasing the cooling rate of the steel side. The welding force and current were fixed as 4.0 kN and 20 kA, respectively, whereas the welding time was

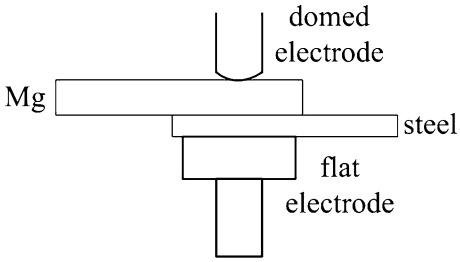

Fig. 3—Schematic diagram of workpieces and electrodes for welding.

changed from one cycle to 16 cycles (60 cycles per second). Four welding samples were made under each welding condition—three for tensile shear test and one for microstructural analysis.

Tensile-shear tests of welds were conducted on an Instron universal test machine (Instron, Norwood, MA) at a constant crosshead speed of 1 mm/min. Special care was taken to minimize the effect of misalignment between the axis of the weld coupons and the loading axis. The thickness of both end sections of the welded specimens was shimmed to the same value as the thickness of the welded region to minimize bending moments. All welded tensile-shear coupons were strained to fracture, and the maximum load was used to indicate the strength of the welds.

After welding, specimens were cut, mounted, polished, and etched. The composition of the etching solution was 20 ml acetic acid, 20 ml water, 3 g picric acid, and 50 ml ethanol. Microstructures and fracture morphology were examined using a JEOL JSM 840 SEM (Japan Electron Optics Ltd., Tokyo, Japan) with 20 kV operating voltage equipped with EDX (Oxford Instruments Microanalysis Group High Wycombe, Bucks, United Kingdom). The phase constitution of fractured joints was analyzed by X-ray diffraction (XRD) analysis using a Rigaku AFC-8 diffractometer with Cu target (Rigaku Corporation, Tokyo, Japan).

III. RESULTS

A. *Mechanical Properties*

Figure 4(a) shows a typical weld cross section. The melted area of magnesium was revealed by etching, and its maximum diameter was defined as D_1. The diameter of the bonded zone on the fracture surfaces was defined as D_2 (Figure 4(b)). The diameter of melted Zn at the steel–electrode interface was defined as D_3 (Figure 4(c)). As shown in Figures 4(b) and (c), no expulsion was observed at either faying surfaces or electrode–workpiece interfaces.

Figure 5 shows the growth of nugget size, fracture surface diameter, and melt Zn diameter (D_1, D_2, and D_3). It shows that all diameters increased with welding time. However, D_2 and D_3 reached a relatively stable level after eight cycles, but D_1 continued to increase with increase of welding time. It also was observed that the order of the three diameters was $D_3 > D_2 > D_1$.

Figure 6 shows the depth of indentation of the magnesium surface. It increased with welding time and

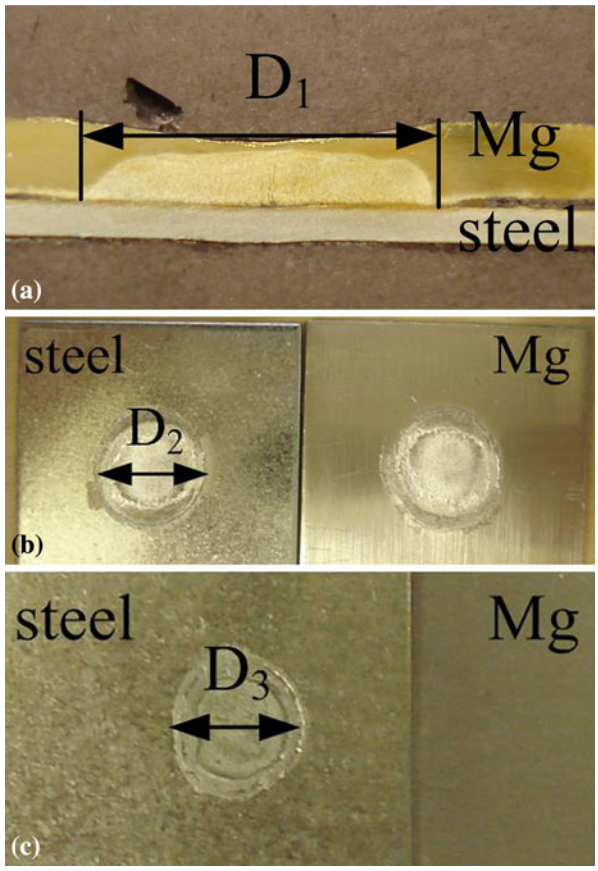

Fig. 4—Measurements of weld dimensions by the following different methods: (*a*) cross section of weld, (*b*) fracture surface, and (*c*) melted zinc at steel–electrode interface.

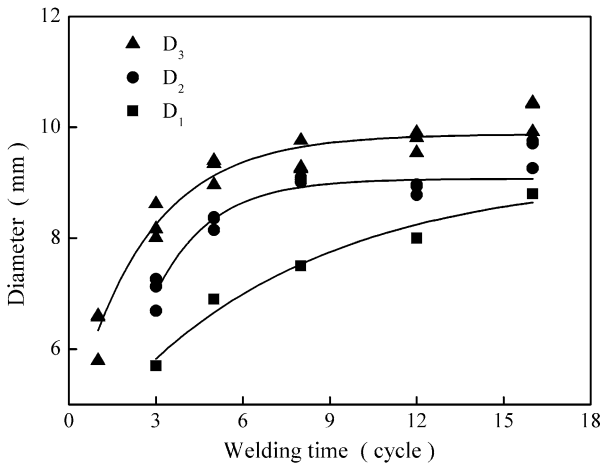

Fig. 5—Growth of weld dimensions with welding time depicting the cross-section nugget size (D_1), fracture surface diameter (D_2), and melt Zn diameter at the steel–electrode interface (D_3).

became constant after eight cycles. The maximum indentation was lower than 10 pct, which is acceptable according to the American Welding Society (AWS) Standard D17.2 for aerospace.[16] The indentation of the steel side was zero even with a welding time of 16 cycles, as expected because of a flat electrode being used.

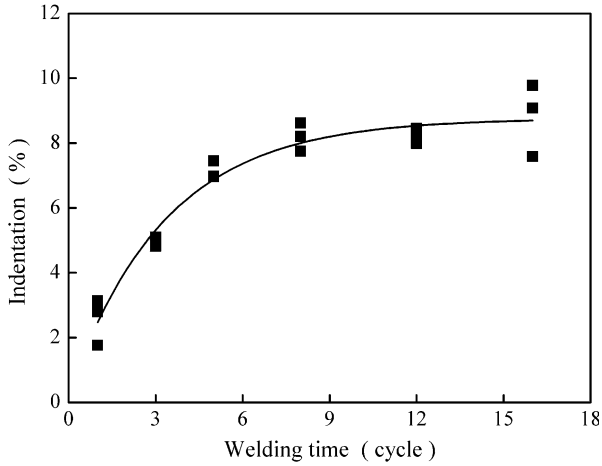

Fig. 6—Indentation *vs* welding time on the magnesium side.

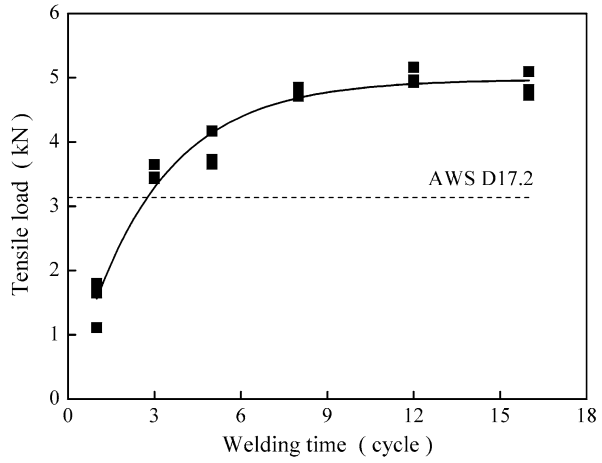

Fig. 7—Tensile-shear strength of magnesium/steel dissimilar welds *vs* the welding time.

Figure 7 shows the relationship between strength and welding time. The strength of the joints increased with welding time and became constant after eight cycles. The strength of welds reached the AWS D17.2 requirement when the welding time was more than three cycles. The largest force was around 5 kN, which was greater than 95 pct of the strength of optimized AZ31B to AZ31B spot joints.[17] All specimens failed in an interfacial failure mode, which indicated that cracks propagated through the fusion zone.

B. *Fracture Morphology*

Figure 8 shows the fracture morphology of a weld with one cycle welding time. Three different kinds of regions were found on both Mg and steel sides, identified in the figures as regions I, II, and A (Figure 8(a)). Region I (Figure 8(b)) had a surface chemistry of 46.3 wt pct Mg and 53.7 wt pct Zn. The free surface of region I indicated that it was formed from liquid melted and squeezed out with a surface morphology imprinted by the Mg as-received surface (Figure 1(b)), and it was not joined to the other side. Region II was the joint area with a diameter of D_2 producing a joint with 1.5 kN strength. The EDX analysis indicated this area comprised about 80 wt pct Zn, 13 wt pct Mg, 5 wt pct Al, and 2 wt pct Fe. It suggests that the Mg and steel sheets were joined (soldered) by molten and resolidified Zn. Small but numerous voids were found on the fracture surface of the joined area (Figure 8(c)), which may be a result of gases trapped between sheets.[18] The details of area A in Figure 8 showed that the bonding was incomplete, with patches of original plating-surface morphology, indicating that these regions were not melted (Figure 8(d)). The tracks in Figure 8(d) were similar to those of the original magnesium surface (Figure 1(b)). This observation suggested that the two areas were in contact with each other during welding. However, because the heat generation was insufficient, they were not melted or joined.

Figure 9 shows the fracture morphology of the Mg side of a fractured joint made with three cycles welding time. Table I summarizes the EDX analysis of different regions. In Figure 9(a), the fracture surface could be divided into the following regions according to their morphology: region I (Figure 8(b)) was smooth, free surface, and the weight percent ratio of magnesium to zinc was about 1:1 (Table I), suggesting it was equivalent to region I of the one-cycle weld. Region II (Figure 9(c)) also had a similar fracture morphology and chemical composition with that of the bond zone at one cycle. The chemical compositions of regions III and IV was the same as AZ31B base material (Table I). Region III looked more dense, and nearly no pores could be found in this region (Figure 9(d)). However, pores were visible in region IV (Figure 9(e)). A clear boundary between regions III and IV was evident on the fracture surface (Figure 9(f)).

Four equivalent regions also were found on the steel side of the fractured three-cycle weld (Figure 10). The morphology and element composition (Table II) of region I on the steel side were similar with those of the Mg side, whereas regions II, III, and IV were different. According to the EDX results, region II was bare steel, indicating fracture of this area occurred at the steel–Zn interface. Black (A) and grey (B) areas were in regions III and IV. The majority element of area A was Mg, whereas in area B, it was Fe. Fracture surfaces of areas A (Figure 10(b)) and B (Figure 10(c)) indicated that the fracture path followed either the Mg–steel interface (area B) or through the Mg fusion zone (area A). It should be noted that the black areas in region III were more extensive than those of region IV, suggesting a better joint strength of Mg to steel in region III.

With a further increase in welding time, the width of region II became narrower from about 450 μm at three cycles to 270 μm at eight and 16 cycles (Figures 9(a), and 11(a) and (b)), and numerous secondary cracks were formed in this region during tensile-shear testing (Figure 11(c)). Pores only rarely were found in the periphery of region IV, which was different from the behavior at three cycles welding time. The strength of these welds became much higher than the standard (3.1 kN).

XRD analyses were performed on the four regions as shown in Figure 12. The majority phases in regions I and II were Mg, Zn, and $MgZn_2$. The intensity of Zn in

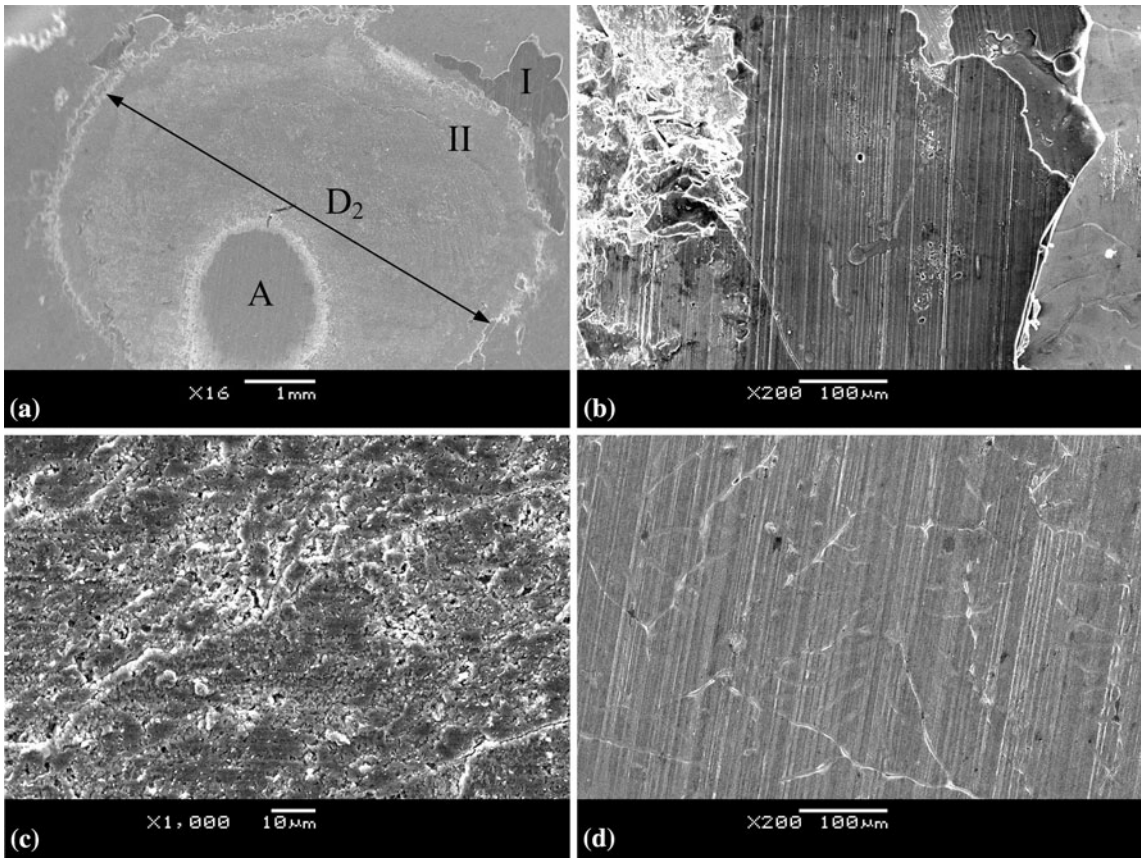

Fig. 8—Fracture morphology of weld with one cycle welding time, at (*a*) steel side; (*b*) details of region I, the squeezed Zn; (*c*) details of region II, the joined area; and (*d*) details of zone A, the unmelted area.

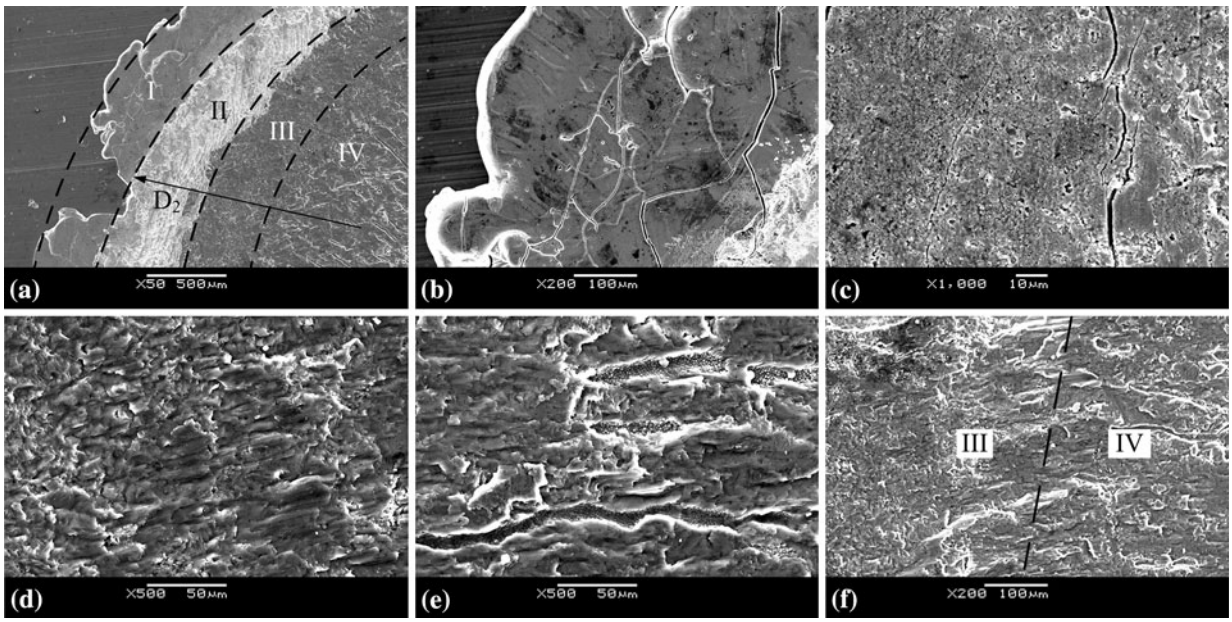

Fig. 9—Fracture morphology of weld made with three cycles at the magnesium side, depicting an (*a*) overview, (*b*) details of region I, (*c*) details of region II, (*d*) details of region III, (*e*) details of region IV, and (*f*) transition from region III to region IV.

region II was higher than region I, and a few $Al_5Mg_{11}Zn_4$ phase particles also were detected in this region. Regions III and IV were almost the same as the Mg alloy base material except for a little $Al_5Mg_{11}Zn_4$, which does not exist in the AZ31B base material. It is believed that the appearance of $Al_5Mg_{11}Zn_4$ phase was a

Table I. Elemental Composition of Different Areas in Figure 9(a) in Wt Pct

Area	Mg	Zn	Al	Fe
I	47.9	50.4	1.6	0.1
II	8.6	90.2	1.2	0
III	96.2	1.1	2.6	0.1
IV	97.6	—	2.4	—

Table II. Elemental Composition of Different Areas in Figure 10(a) in Wt Pct

Area	Mg	Zn	Al	Fe	Cr	Mn	C
I	48.9	51.1	—	—	—	—	—
II	—	5.6	10.9	80.9	1.0	1.6	—
A in III	97.9	—	2.1	—	—	—	—
B in III	34.5	—	8.7	51.7	—	—	5.1

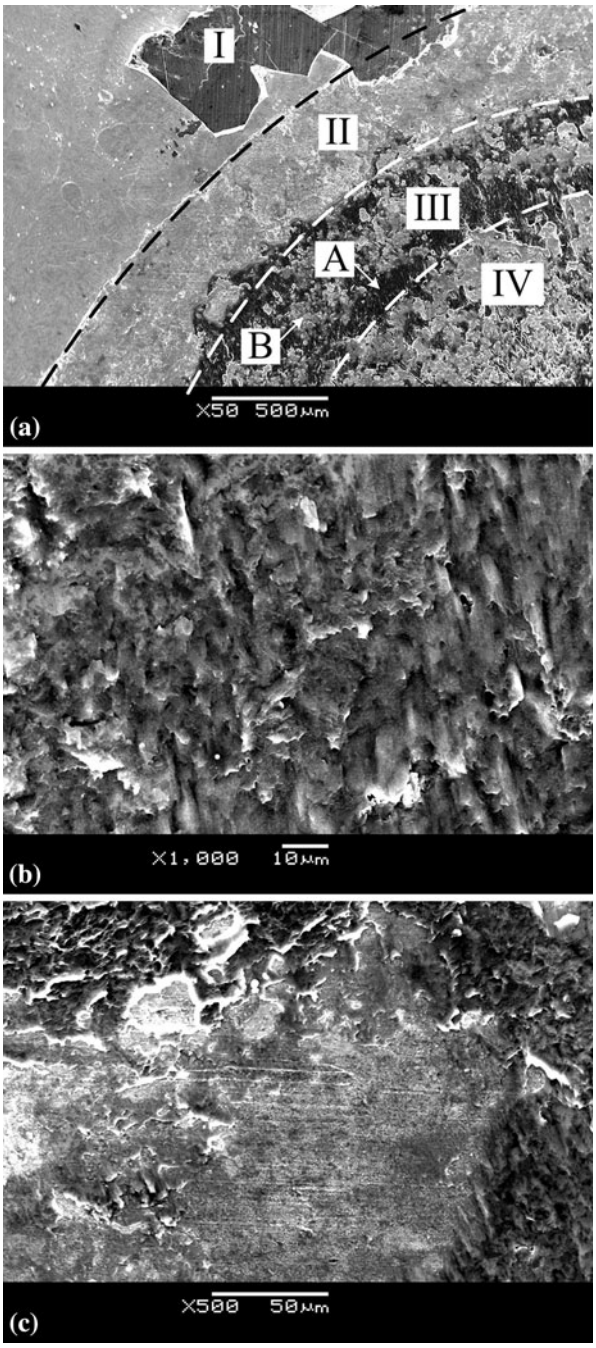

Fig. 10—Fracture morphology of weld made with three cycles at steel side, depicting (*a*) an overview, (*b*) details of area A, and (*c*) details of area B.

result of the dissolution of extra Zn into the Mg welding pool. No large amount of brittle Mg-Zn phase was formed in the nugget because most of the the zinc layer was squeezed out of the central nugget region and deposited as regions I and II.

C. *Microstructures*

Figure 13 shows a cross section of magnesium to steel welded with three cycles. Three regions with different morphologies and compositions also were found along the Mg–steel interface that correspond to the fracture surface features discussed (Figure 9(a)). Region II consisted of two solder layers (because the melting temperature is less than 723 K (450 °C)[18]) that were characterized by different chemical compositions and marked as B and C. Layer B consisted of 12.4 wt pct Mg and 87.6 wt pct Zn (Table III), which was similar to that of region II of fracture surfaces (Figures 8(c) and 9(b)) and should contain a similar phase composition. In layer C, the ratio of Mg to Zn was 1:1, which was the same as that observed in region I in Figures 8(b) and 9(b). Equiaxed grains were found in region III (Figure 12(c)), the size of which was larger than those of the base material. So it is believed that in region III, magnesium was melted partially, and the joint really is formed by a combination of solid-state and fusion bonding. Region IV was in the center of the Mg fusion zone (*i.e.*, D_1), as shown in Figure 4(a). In region IV, magnesium alloy was melted and was braze-welded to steel. As to the solidification morphology of the steel side, no melt was found even in the center of the nugget.

Figure 14 shows the microhardness distribution along the center of a weld made at 16 cycles. On the magnesium side, hardness was highest at the interface and decreased along the thickness direction. However, on the steel side, the highest hardness area was between the interface and the center of the sheet. It is believed that the enhanced hardness of the Mg side was a result of alloy strengthening, and the area near the interface had more alloying elements. Because the electrical conductivity of steel is much lower than magnesium,[9] the heat generation on the steel side would be higher than that on the magnesium side. The steel then could serve as a hot anvil to heat the magnesium. Because of the heat losses from both magnesium and electrode/steel, the highest temperature occurred in the center of the steel thickness, which could promote martensite transformations, increase the martensite content, and then lead to higher local hardness.[19,20]

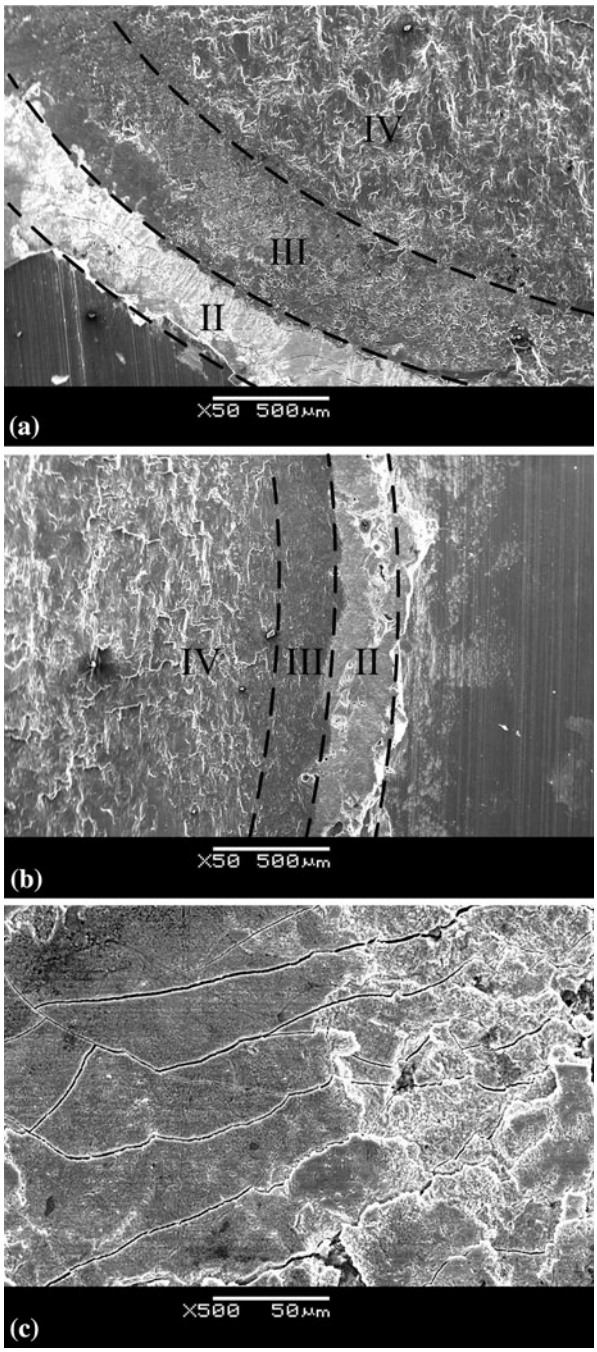

Fig. 11—Fracture morphology of magnesium side at (*a*) eight cycles, (*b*) 16 cycles, and (*c*) details of region II in eight cycles.

IV. DISCUSSION

The dissimilar joining of AZ31 to DP600 is discussed in this section under the following topics: the mechanisms of joint formation and the effects of the Zn soldering layer on the weld strength. A comparison of Mg/steel with Zn-coated-steel/Zn-coated-steel,[21] Au-plated-Ni, and bare-Ni/bare-Ni are discussed.[18] A possible expansion of this technology also is discussed.

A. *Joint Formation*

A schematic diagram of joint formation is provided to assist the following discussion (Figure 15). In the first stage of welding (Figure 15(a)), Mg and steel sheets are soldered together by the Zn layer on the steel surface. The contact resistance of the faying surface initially will be higher because of the presence of surface oxides. So, heat generation at the faying surface initially would be higher than in the bulk material. For a short welding time, a nonwelded region may appear in the middle of the spot, as shown in Figure 8(d). A similar phenomenon was found in RSW of steel with a short welding time[22] because resistance heating was most intense close to the periphery of the contact area, causing the temperature of this region to rise sharply.[23] However, even the donut-shaped soldered joint can produce significant strength, about 1.5 kN, as shown in Figure 7. According to the Mg-Zn binary-phase diagram on the freezing of eutectic alloys, the formation of Mg_2Zn_{11} is suppressed sometimes, and a metastable eutectic structure, $MgZn_2$ + (Zn), forms before the melting of the Mg base material, which has been confirmed by the XRD data from region II.

With subsequent heating, the zinc layer is melted completely, and the shape of the fusion zone changes from donut to circle, as shown in Figure 15(b). The magnesium near the interface begins to dissolve in the zinc, but the bulk material is still solid and no melting of magnesium occurs because the melting point of Mg base material is higher than that of Zn or Mg-Zn phases. Because of the electrode force, liquid Zn and $MgZn_2$ are squeezed out, and magnesium directly touches bare steel (Figure 15(c)). The elemental composition in regions III and IV is the same as AZ31B base material, and the XRD results show that they mainly consist of Mg and very few particles of $Al_5Mg_{11}Zn_4$. So it could be concluded that most of the Zn is squeezed out to the peripheral region (regions I and II in Figures 9(b) and (c)) of the nugget at the third stage. Because of the nonuniform thermal expansion, a gap between the Mg and steel sheets is formed around the joined area.[24]

With Zn being squeezed out, solid-state bonding occurs at the center (region III) because no melting of magnesium was observed. As pointed out by many researchers, temperature, pressure, and surface condition are the most important factors for solid-state joining.[25] In the present study, the pressure applied by the weld force is about 50 MPa to 140 MPa. The bare steel surface is very clean from the protection of the Zn coating before welding and the cleaning effect during welding. Moreover, the interface of steel and Mg is sealed mechanically by the squeezed zinc during welding; therefore, no metallic oxides could be formed during welding. All these elements create a condition similar to diffusion welding in a vacuum chamber. As a result, a high bond strength could be obtained.

In the fourth stage, the Mg alloy, which contacts bare steel directly, starts melting by heat flow from the steel side and its own joule heat, as shown in Figure 15(d). The solid-state joint of region III protects the weld pool

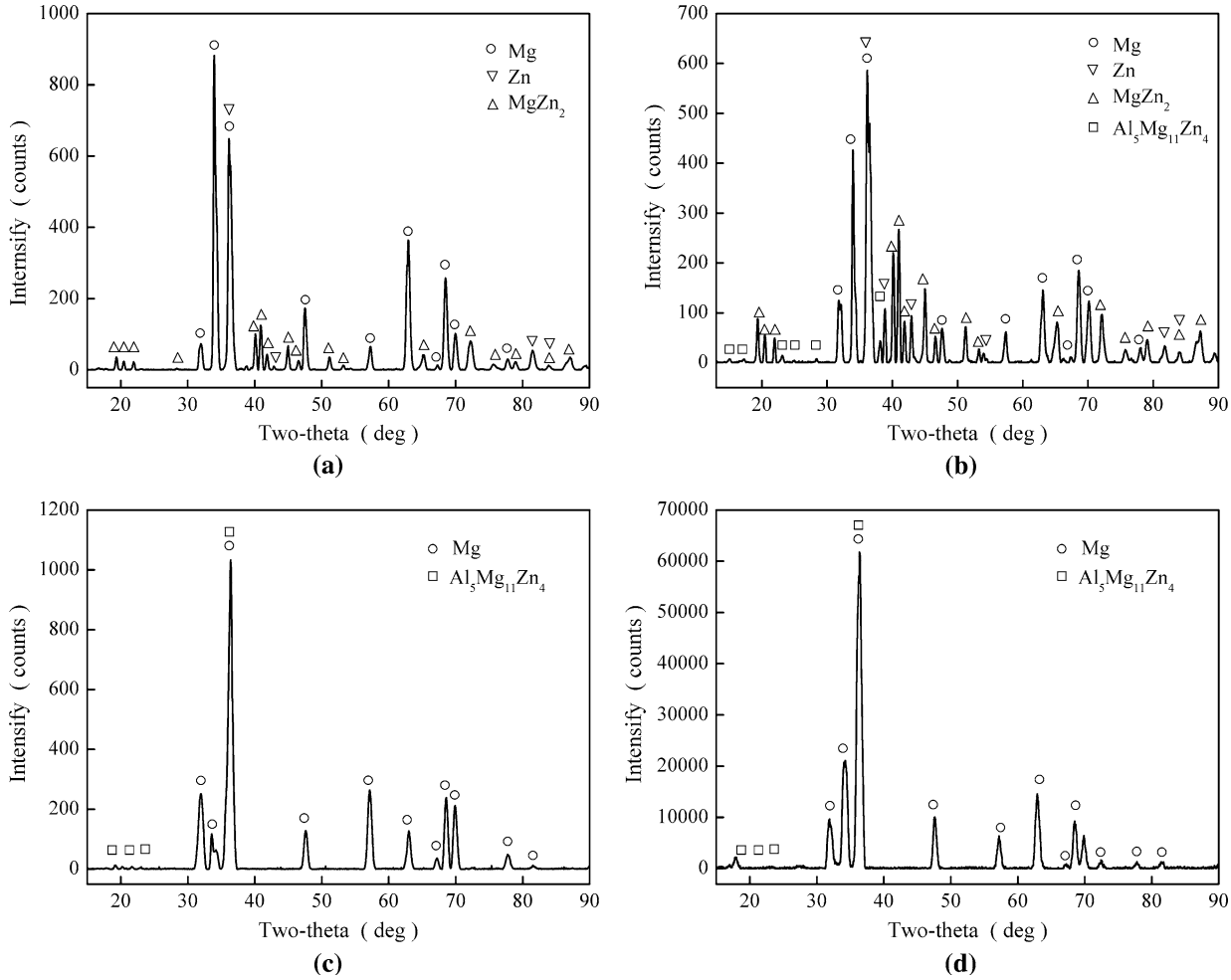

Fig. 12—XRD analysis of different regions of fracture surface in Figure 9, depicting (*a*) region I, (*b*) region II, (*c*) region III, and (*d*) region IV.

away from expulsion. In the end, a hat-shape joint area is formed with high strength, as shown in Figure 15(d). With further increase of the welding time, the area of melted magnesium increases, and the nugget grows bigger, as shown in Figure 15(e). Regions II and III become narrow, and region IV grows bigger. D_1 and D_2 are closer to each other.

Similarities of joining phenomena are found between RSW of Zn-coated steel/steel and steel/Mg, in particular the squeezing out of Zn in the early stage of the process. The difference is whether steel is melted. A liquid weld pool (nugget) forms during the welding of steel/steel. But in the current work, the clean and mechanically sealed steel is not melted, which provides an ideal condition for wetting and solid-state bonding. The Zn coating would not significantly influence the strength of fusion welds like steel–steel,[21] but it has great effects on braze welding and solid-state bonding in this dissimilar metal application. This technology also can be expanded as follows to flux-free braze welding using RSW: precoating of low melting point metal to protect the surface; the coating melts before the melting of the base material; the coating is squeezed out and mechanically seals the brazing area during the joining process.

B. *Bonded Area and Joint Strength*

The shape and size of a nugget play an important role in the strength of welds. In this work, donut-shape joints were produced at a short welding time, and a hat-shape joint resulted from a long welding time. The joint could be divided into four regions; regions II to IV contribute to the strength of welds, but region I does not. Every region produces different microstructures, phases, and chemical compositions. Region IV was the center area of the nugget, in which magnesium was melted, and pores and cracks are found frequently in this region. However, nearly no defects were found in region III, which had a microstructure similar to a partially melted zone. Outside of region III is region II, which was filled by squeezed Zn. So from the view of joining mechanisms, region IV was formed by weld brazing of Mg to steel, region III contained a combination of solid-state bonding and brazing of Mg to steel, and region II was formed by the soldering of magnesium to steel by the zinc-based filler material Zn97Fe3 (Zn coating, with 97 wt pct Zn and 3 wt pct Fe).

In RSW of Mg or Al alloys, a plastically deformed ring, in which solid-state bonding occurs, generally can be found.[26] But the strength of those solid-state bonded

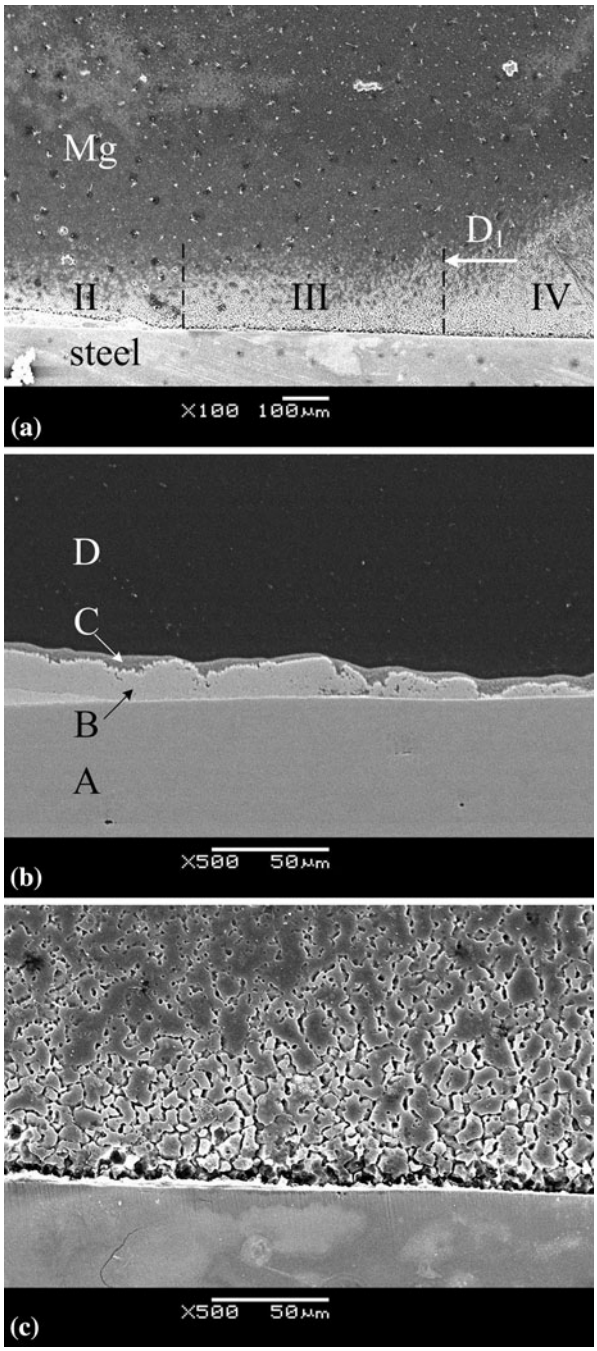

Fig. 13—Interface of magnesium to steel weld with three cycles welding time depicting (*a*) overview, (*b*) details of region II, and (*c*) details of region III.

Table III. Elemental Composition of Different Areas in Figure 13(b) in Wt Pct

Area	Mg	Al	Fe	Zn
A	—	—	100	—
B	12.4	—	—	87.6
C	50.1	—	—	49.9
D	96.5	3.5	—	—

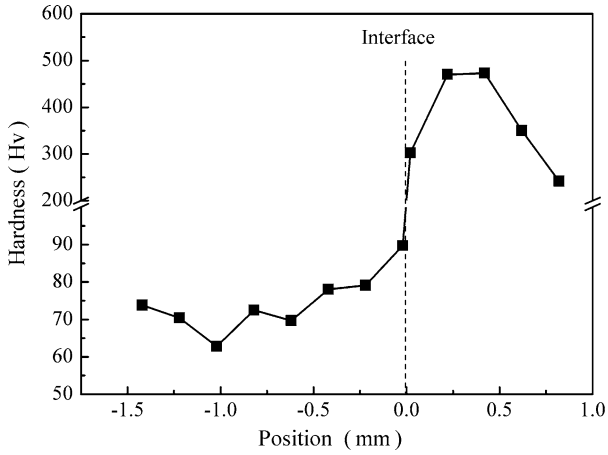

Fig. 14—Hardness distribution along the thickness direction welded with 16 cycles.

zones is weaker compared with the fusion zone. So nugget size always is defined as the diameter of the fusion zone, and the width of the external plastic ring is not included in the nugget diameter to evaluate the weld strength. Generally, with an interfacial failure mode, the joint strength increases with nugget diameter, and it becomes stable if the nugget diameter does not change. In the current work, after eight cycles, D_2 and weld strength simultaneously became stable, whereas D_1 kept increasing. This observation suggests that the strength of welds mainly was related to D_2 and not D_1. The definitions of diameters D_1 and D_2 reflect the characteristics of regions II and III, which were formed by soldering and solid-state bonding, respectively. The joint strength was 1.5 kN with soldering only in one cycle of heating. The solid-state bonding provided better strength than fusion bonding according to the fracture surface on the steel side (Figure 10). In the literature, Zn also has been used as an interlayer to bond Mg and Al alloys.[27,28] Even without the formation of a fusion nugget, solid-state bonds of Au-plated Ni sheets can be stronger than the bare Ni joints with a nugget.[18] So regions II and III would have great effects on the strength of welds, and it therefore makes sense to add both the fusion zone and the solid-state bonded area as the "bond diameter." Region II seems to be particularly important to the weld integrity because of the existence of a high stress concentration in this region.

V. CONCLUSIONS

AZ31B/steel dissimilar joints were formed successfully by RSW. The optimum strength of the welds was 5.0 kN, which is about 95 pct of that of an optimized Mg/Mg joint. The major conclusions are summarized as follows:

1. A hat-shaped joint was formed during RSW of magnesium to zinc-coated steel. The joint areas could be divided into the following regions from

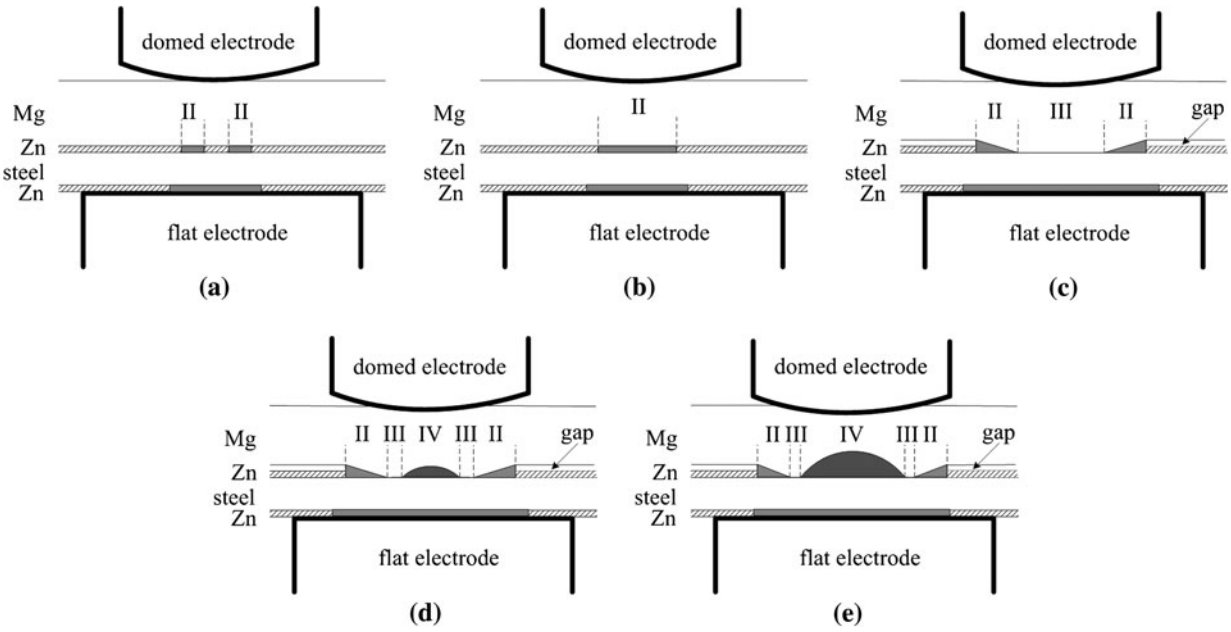

Fig. 15—Sechematic diagram of joint formation during welding of mangesium to steel sheets, depicting (*a*) melting initiates at Mg–Zn interface with a donut shape, (*b*) totally melting of Zn and soldering of Zn to Mg, (*c*) squeezing Zn out, (*d*) melting and brazing of Mg to steel, and (*e*) growth of the nugget.

outside to the center: soldering of magnesium to steel by zinc-based filler (region II): solid-state bonding of magnesium to steel (region III); weld brazing of magnesium to steel in the center of the weld with certain penetration (region IV). Zinc was squeezed out of the fusion zone and formed region II, which mechanically could seal the nugget. The fresh and intact steel surface could produce an ideal condition for the wetting of magnesium to steel in region IV and solid-state bonding in region III.

2. The diameter of fracture surfaces (D_2) and the strength of welds increased with welding time and became stable after eight cycles, whereas the diameter of fusion zone (D_1) kept increasing up to 16 cycles. The difference between D_1 and D_2 was the existence of regions II and III, which have great influence on the strength of welds.
3. Use of a radiused electrode against the Mg sheets and a flat electrode against the steel surface was needed to keep the temperature of steel below its melting point. The hardness near the bonded interface of the steel side was lower than the center of the sheet thickness, suggesting that steel served as a heat generator at the later stages of the welding process because of its large bulk resistance.

ACKNOWLEDGMENTS

This research was supported financially by the Natural Sciences and Engineering Research Council (NSERC) of Canada, AUTO21 Network Centres of Excellence of Canada, and NSERC Magnesium Network (MagNET). The authors want to thank Professors S. Lawson, G.S. Zou, and L.Q Li for their suggestions in this work and also are grateful for the materials support of POSCO.

REFERENCES

1. L.M. Liu, G. Song, and M.L. Zhu: *Metall. Mater. Trans. A*, 2008, vol. 39A, pp. 1702–11.
2. S.C. Park, Y.S. Sato, and H. Kokawa: *Scripta Mater.*, 2003, vol. 49, pp. 161–66.
3. L.M. Liu, G. Song, G.L. Liang, and J.F. Wang: *Mater. Sci. Eng. A*, 2005, vol. 390, pp. 76–80.
4. L. Liu, S.Q. Zhou, Y.H. Tian, J.C. Feng, J.P. Jung, and Y. Zhou: *Sci. Technol. Weld. Join.*, 2009, vol. 14, pp. 356–61.
5. T. Watanabe, K. Kagiya, A. Yanagisawa, and H. Tanabe: *Quart. J. Jpn. Weld. Soc.*, 2006, vol. 24, pp. 108–15.
6. Y.C. Chen and K. Nakata: *Mater. Des.*, 2009, vol. 30, pp. 3913–19.
7. L.M. Liu and X. Zhao: *Mater. Character.*, 2008, vol. 59, pp. 1279–84.
8. X.D. Qi and G. Song: *Mater. Des.*, 2010, vol. 31, pp. 605–09.
9. J.C. Feng, Y.R. Wang, and Z.D. Zhang: *Sci. Technol. Weld. Join.*, 2006, vol. 11, pp. 154–62.
10. D.Q. Sun, B. Lang, D.X. Sun, and J.B. Li: *Mater. Sci. Eng. A*, 2007, vols. 460–461, pp. 494–98.
11. L. Xiao, L. Liu, Y. Zhou, and S. Esmaieli: *Metall. Mater. Trans. A*, 2010, vol. 41A, pp. 1511–22.
12. T. Watanabe, A. Yanagisawa, S.K. Ma, and Y. Doi: *Weld. Inter.*, 2005, vol. 23, pp. 491–95.
13. R.F. Qiu, C. Iwamoto, and S. Satonaka: *Mater. Character.*, 2009, vol. 60, pp. 156–59.
14. X. Sun, E.V. Stephens, M.A. Khaleel, H. Shao, and M. Kimchi: *Weld. J.*, 2004, vol. 83, pp. 188s-95s.
15. Method and Material for Resistance Welding Steel-Base Metal Sheet to Aluminum-Base Metal Sheet, Patent U.S. Application 5 783 794.
16. AWS D17.2, Specification for Resistance Welding for Aerospace Applications, 2007.

17. S.Q. Zhou, L. Liu, J.P. Jung, M.Y. Lee, and Y. Zhou: *Metal. Mater. Inter.* Under review.
18. W. Tan, Y. Zhou, and H.W. Kerr: *Metall. Mater. Trans. A*, 2002, vol. 33A, pp. 2667–76.
19. M. Xia, E. Biro, Z. Tian, and Y. Zhou: *ISIJ Int.*, 2008, vol. 48, pp. 809–14.
20. V.H. Baltazar, M.L. Kuntz, M.I. Khan, and Y. Zhou: *Sci. Technol. Weld. Join.*, 2008, vol. 13, pp. 769–76.
21. S.A. Gedeon and T.W. Eagar: *Metall. Trans. B.*, 1986, vol. 17B, pp. 887–901.
22. S.I. Rokhlin and L. Adler: *J. Appl. Phys.*, 1984, vol. 56 (3), pp. 726–31.
23. J.A. Greenwood and J. Williamson: *Proc. R. Soc. London*, 1958, vol. 264A, pp. 13–31.
24. B.H. Chang, M.V. Li, and Y. Zhou: *Sci. Technol. Weld. Join.*, 2001, vol. 6, pp. 273–80.
25. A. Hill and E.R. Wallach: *Acta Mater.*, 1989, vol. 37, pp. 2425–37.
26. Y.R. Wang, J.C. Feng, and Z.D. Zhang: *Sci. Technol. Weld. Join.*, 2006, vol. 11, pp. 555–60.
27. L.M. Zhao and Z.D. Zhang: *Scripta Mater.*, 2008, vol. 58, pp. 283–86.
28. L.M. Liu, L.M. Zhao, and R.Z. Xu: *Mater. Des.*, 2009, vol. 39, pp. 4548–51.